BULLETIN OF THE POLISH ACADEMY OF SCIENCES
TECHNICAL SCIENCES, Vol. 69(1), 2021, Article number: e136190
DOI: 10.24425/bpasts.2021.136190

A decentralized control strategy to bring back frequency and share reactive power in isolated microgrids with virtual power plant

Amir KHANJANZADEH, Soodabeh SOLEYMANI*, and Babak MOZAFARI

Electrical and Computer Engineering Department, Science and Research Branch, Islamic Azad University, Tehran, Iran

Abstract. In this paper, a novel Power-Frequency Droop Control (PFDC) is introduced to perfectly bring back the system frequency and share the reactive power in isolated microgrid with virtual power plant (VPP). The frequency-based power delivery must be essentially implemented in VPP which can operate as a conventional synchronous generator. It has been attained by enhancing the power processing unit of each VPP to operate as an active generator. The inverter coupling impedance which has been assigned by the virtual impedance technique has reduced the affected power coupling resulting from line resistance. The reference has been subsequently adjusted to compensate the frequency deviation caused by load variation and retrieve the VPP frequency to its nominal value. In addition, the line voltage drop has compensated the voltage drop and load sharing error to obliterate the reactive power sharing imprecision resulting from the voltage deviation. The voltage feedback confirms the correct voltage after compensating the voltage drop. As an illustration, conventional PFDC after a load change cannot restore the system frequency which is deviated from 50 Hz and rested in 49.9 Hz while, proposed PFDC strategy fades away the frequency deviation via compensating the variation of the frequency reference. Likewise, the frequency restoration factor (γ) has an effective role in retrieving the system frequency, i.e., the restoration rate of the system frequency is in proportion with γ. As a whole, the simulation results have pointed to the high performance of proposed strategy in an isolated microgrid.

Key words: PFDC; VPP; microgrid; virtual impedance; decentralized control.

1. Introduction

Due to the environmental anxieties regarding pollution, species extinction, climate changes, deposit acid and suchlike, the increasing efforts to decrease the carbon emissions from the energy sector has created an all-round interest in renewable energy and related technologies, which has led to progress and innovation of renewable based technologies [1]. The continued growth of scientific endeavors in this field leads to incremental installations of Renewable Energy Sources (RESs) such as Wind Turbine (WT), Photovoltaic (PV), Fuel Cell (FC), and Battery Energy Storage (BES) accompanied by providing exceptional opportunities for cost-effective load schedule and demand response program [2–4]. Microgrid including these resources has provided a reliable electrical power for sensitive loads via large integrated VPP [5, 6].

According to the synchronous generator features, the PFDC is suggested to be applied for isolated microgrid as well as VPP control in the decentralized peer to peer control structure. Due to the dominance of the short transmission line resistance, power coupling problem appears during PFDC operation [7, 8]. Hence, it is very likely that the transient and dynamic operative condition of microgrid to be broken down [9]. An extra inductor can be added to the transmission line, and Virtual Impedance Technique (VIT) decouples the active and reactive power to accurately share the power and enhance the system stability toward utilizing the PFDC for low voltage microgrid [10, 11]. Due to proportionate output active power of VPP with the system frequency, load changes and perturbations can deviate the frequency from its operational value. Hence, the frequency deviation turns to be an eminent issue for droop control-based isolated microgrid [12, 13].

As a consequence, it can decrease the power quality, power system stability, load availability and electricity customer service [14, 15]. However, a trivial deviation appears in voltage caused by line voltage drop. Due to mismatch in impedance of transmission lines, and their subsequent voltage drop has created voltage deviation. Therefore, the reactive power has not been accurately exchanged according to the rate of droop factors. Inaccurate share of the reactive power has not provided nominal active and reactive power for loads and steady-state and dynamic stability for VPP accompanied by its relevant electrical efficiency [16].

Centralization of the constructed microgrid is feasible through communication links to exchange the control signals between power system and renewable resources, i.e., collecting the information from the power system and dispatching the required command to VPPs toward control of microgrid. Despite that, decentralized droop control strategy will be more efficient and applicable during absence or viability of the communication links [17]. Due to the direct controllability of droop control with the shared power with respect to RESs based on apparent power ratings, decentralized control approaches have autonomously operated with lack of communication link, and accordingly enhance the reliability with more simplification, whereas many drawbacks and problems will be revealed [18–20].

*e-mail: s.soleymani@srbiau.ac.ir

Manuscript submitted 2020-05-22, revised 2020-08-05, initially accepted for publication 2020-11-05, published in February 2021

Since the previous approaches necessitate the communication link to support the required coordination among RESs, different centralized and distributed coordination control strategies have been schemed and proposed for microgrids in [21–30], that contain: unity synchronous control owing to the state-feedback controller [21–24], the distributed cooperative-adaptive voltage-frequency controller [25, 26], the centralized compensative controller [27, 29], and synchronous signal-producing controller [30]. To attain almost independent communication, event triggered-communication strategy [31], two-layer intermittent-communication strategy [32], and the sparse-communication strategy [33] have been suggested. Even though the accurate control has been attained during lower communication application and feasible communication deterioration, but disruption in control strategies in [21–30] can be appeared that decentralized control strategy has to be considered. The droop controller has been directly ameliorated to refrain from creating the communication-link. Hence, VPP necessitates the relevant information concerned itself. Control strategies suggested so far include conventional decentralized secondary voltage-frequency control strategy with regard to adaptive state estimator [34], the reactive power sharing control strategy with regard to voltage compensation [35], dynamic state estimator with respect to nonlinear particle filter [36], voltage drop compensation using adaptive virtual impedance strategy [37], and virtual negative impedance control strategy [38]. As a consequence, decentralized control strategy has effectually ameliorated the reliability, self-adaptability and upgradeability of microgrid.

In this paper, a novel decentralized control strategy is proposed accurately restore the frequency and share the reactive power in isolated microgrids with VPPs. By adjusting the frequency reference signal via compensating the line voltage drop toward enhancement of the voltage droop factor, and also incorporating the output voltage feedback at terminal of the voltage droop, PFDC structure has conclusively upgraded. The voltage droop factor has been enhanced via compensating the line voltage drop, and reactive power has been accurately shared during the unchanged states with existence of the voltage difference. The exactness of reactive power sharing strategy will be guaranteed by output voltage feedback loop that the relevant feedback reference has been attained with in accordance with the required reactive power.

2. Consideration of inverter coupling impedance to construct droop control of power-frequency

Figure 1 presents the equivalent circuit of the understudy power system. The output voltage is indicated by $E\angle\delta$, where, $E_S\angle 0$ indicates the sending-bus voltage. S, P and Q respectively indicate the output apparent, active and reactive powers provided by VPP, and i_L indicates the line current. Z_L and Z_I are respectively the line impedance and the inverter coupling impedance. The inverter links the VPP to the microgrid. The value inverter coupling impedance has been tuned by virtual impedance technique.

The output active and reactive powers of a VPP are given as follows:

$$\begin{cases} P = \left[E^2\cos(\varphi) - EE_s\cos(\varphi+\delta)\right]Z^{-1} \\ Q = \left[E^2\sin(\varphi) - EE_s\sin(\varphi+\delta)\right]Z^{-1} \end{cases} \tag{1}$$

where, $Z = Z_L + Z_I$. It is worth mentioning, the perturbation of ΔE and $\Delta\delta$ in the equilibrium point (E_e, δ_e) causes the output power variation. Linearizing Eq. (1) leads to:

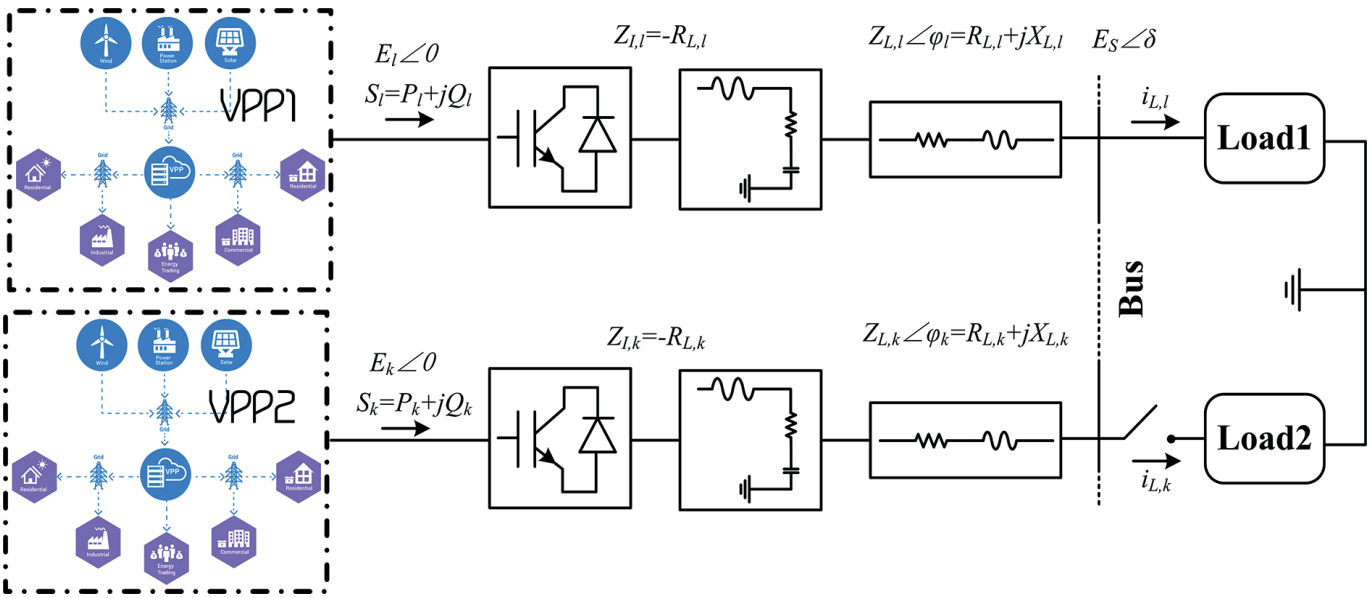

Fig. 1. Network equivalent circuit with impedances of inverter coupling and line

$$\begin{cases} \Delta P = \left[\partial P/\partial \delta\right]\Delta\delta + \left[\partial P/\partial E\right]\Delta E \\ \Delta Q = \left[\partial Q/\partial \delta\right]\Delta\delta + \left[\partial Q/\partial E\right]\Delta E \end{cases} \tag{2}$$

where:

$$\begin{cases} \partial P/\partial\delta = E_s E_e \sin(\varphi + \delta_e) Z^{-1} \\ \partial P/\partial E \approx \left[\left[2E - E_s\right]\cos\varphi\right] Z^{-1}\Big|_{\delta_e \approx 0} \\ \partial Q/\partial\delta = -E_s E_e \cos(\varphi + \delta_e) Z^{-1} \\ \partial Q/\partial E \approx \left[\left[2E - E_s\right]\sin\varphi\right] Z^{-1}\Big|_{\delta_e \approx 0}. \end{cases} \tag{3}$$

As for Eq. (3), $\partial P/\partial E$ and $\partial Q/\partial\delta$ are highly sensitive due to low value of φ in low voltage microgrid. That is to say, there is a solid link between both the active and reactive powers in PFDC strategy. According to Fig. 2, considering $0° < \varphi < 90°$, the variations of frequency and voltage have respectively affected the reactive and active power, and present the power coupling. The active and reactive power respectively depend on the voltage and frequency with $\varphi = 90°$ and present the power decoupling. Since φ plays an important role in power coupling, the inverter coupling impedance has been applied to adjust φ to 90° in low voltage microgrid.

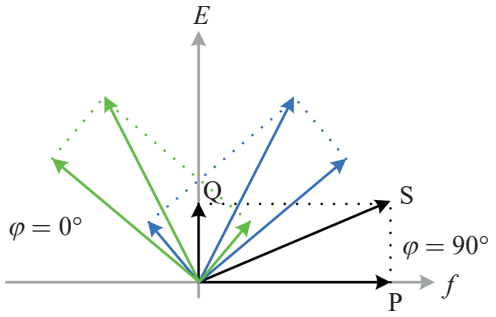

Fig. 2. Variations of power coupling with different angles for line impedance

There are two alternatives to decrease the line resistance, adding: high virtual inductance and high negative virtual resistance. Note that, the additional inductance can create undesired harmonics [19]. Hence, the inverter coupling impedance must be tuned based on the negative virtual resistance, i.e.:

$$Z_I = -R_L. \tag{4}$$

However, the resistance of short transmission line has been removed, and the short-transmission line becomes inductive. Since the value of δ is very small and φ becomes 90°, thus:

$$\begin{cases} \cos(\varphi + \delta) = -\sin\delta \approx -\delta \\ \sin(\varphi + \delta) = \cos\delta \approx 1. \end{cases} \tag{5}$$

Substituting Eq. (5) in Eq. (1) leads to:

$$\begin{cases} \delta = \left(\dfrac{X_L}{E_s E}\right).P \\ E - E_s = \left(\dfrac{X_L}{E_s E}\right).Q. \end{cases} \tag{6}$$

Deriving the voltage difference between VPP_i and VPP_j becomes $\Delta E = (\Delta X_L \cdot \Delta Q)/E_S$. Discarding the inverter coupling impedance results in $\Delta E' = (\Delta X_L \cdot \Delta Q + \Delta R_L \cdot \Delta P)/E_S$. According to the line types in low voltage microgrid, the resistive part is more varied as compared to inductive part, i.e., $\Delta R_L \gg \Delta X_L$, in such a way $\Delta E' > \Delta E$. So, the reactive power has been inaccurately shared. If VPP_i and VPP_j have same capacity, then $\Delta E' = \Delta E$ due to the continual and accurate share of the active powers, i.e., $\Delta P = 0$ while, the reactive power has been shared with the continual accuracy. That is to say, the inverter coupling impedance can cause accurate sharing of the reactive power.

Based on PFDC, Eq. (6) can be represented as follows:

$$\begin{cases} f = f_n + \alpha P \\ E = E_n + \beta Q \end{cases} \tag{7}$$

where, f_n, E_n are respectively the rated frequency and voltage references, and α, β are respectively the frequency and voltage droop factors.

$$\begin{cases} \alpha = \dfrac{(f_{\min} - f_n)}{P_{\max}} \\ \beta = \dfrac{(E_{\min} - E_n)}{Q_{\max}} \end{cases} \tag{8}$$

where, $f_{\min}$ and $E_{\min}$ respectively indicate the minimum frequency and voltage of VPP, also, $P_{\max}$ and $Q_{\max}$ respectively indicate the maximum active and reactive power of VPP.

3. Suggested frequency restoration strategy

By detecting the variation of active power in VPP using Wavelet Transform (WT), the frequency deviation can be attained. The required reference has compensated the frequency deviation to restore the frequency, and also it can be promptly restored via assigning the exponential reduction mode of the frequency deviation.

3.1. Frequency reference variation. Figure 3 presents the curve of frequency droop, and l_o indicates the conventional droop curve that changes to l_1 or l_2 during the reference variation. $f(t)$ and $P(t)$ respectively indicate the frequency and output active power of V The frequency deviation is defined by, and its relevant variation is, $f_n(t)$ indicates the frequency reference.

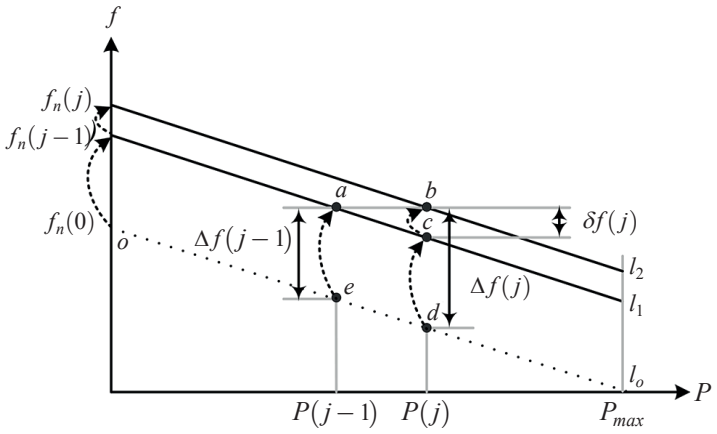

Fig. 3. Characteristic of frequency variation in frequency droop control

As for the l_o, the frequency in e and d points deviates from the nominal value with respective frequency deviations $\Delta f(j-1)$ and $\Delta f(j)$ during the variation of the active power to $P(j-1)$ and $P(j)$. Hence, the frequency deviation has proportionally related to the active power. Thus, a decentralized frequency restoration control strategy is proposed for VPP.

The active power variation must be promptly and reliably detected to accurately restore the frequency. Due to instantaneous detection of the signal variation by WT, it has been commonly implemented to detect the parameter variation in the microgrid [39]. A continuous wavelet transforms (CWT) for $P(t)$ at translating factor β and scaling factor α can be presented as follows [34]:

$$W_{\alpha,\beta}(t) = \frac{\int P(t)\psi(t-\beta)\alpha^{-1}.dt}{\sqrt{|\alpha|}} \tag{9}$$

$\psi(t)$ indicates the wavelet function. CWT coefficients have been separated using $P(t)$, and can be presented as follows:

$$C(\alpha,\beta) = \int P(t)W'_{\alpha,\beta}(t).dt. \tag{10}$$

These coefficients have been promptly increased with small value during variation of $P(t)$. Being greater than a particular threshold, detection of the variable has been performed. Even so, a low perturbation in power can lead to the miscalculation in spite of the absence of variation in power. ±1% threshold of active power is defined according to the admissible magnitude variation of power perturbation. It must be considered that the variation in active power that the magnitude becomes over than higher threshold has been figured out.

No assuming the demand at initial instant and active power variation at t = 1, ···, j, ···, n(j ≥ 2), the active power variation set can be presented by following matrix:

$$A = \left[\Delta P(0) \cdots \Delta P(j) \cdots \Delta P(n)\right]^T \tag{11}$$

where, $\Delta P(j) = \Delta P(j) - P(j-1)$ indicates the active power variation which is identified by CWT at t = j. As for Eq. (7), $\delta f(t)$ at the same time can be given as follows:

$$\delta f(j) = m.\Delta P(j). \tag{12}$$

The matrix of frequency reference variation considering $\Delta f_n(0) = 0$ is given as follows:

$$B = -mA = \left[\Delta f_n(0) \cdots \Delta f_n(j) \cdots \Delta f_n(n)\right]^T \tag{13}$$

where, $\Delta f_n(j) = f_n(j) - f_n(j-1) = -\delta f(j)$ to counteract $\delta f(j)$ identifies the value of frequency reference variation at t = j.

The matrix of frequency references considering the initial frequency $f_n(0) = 50$ is given as follows:

$$F = \left[f_n(0) \cdots f_n(j) \cdots f_n(n)\right]^T. \tag{14}$$

In accordance with Eq. (11–14), Eq. (15) will be:

$$(C - E)F = mA \tag{15}$$

where, E indicates the unit matrix, and C indicates the constant matrix:

$$C = \begin{bmatrix} 1 & 0 & \cdots & 0 & 0 \\ 1 & 0 & \cdots & 0 & 0 \\ \vdots & & \cdots & 0 & 0 \\ \vdots & \vdots & \ddots & 0 & 0 \\ 0 & 0 & \cdots & 1 & 0 \end{bmatrix}_{(n+1)\times(n+1)}. \tag{16}$$

The varying frequency reference parts have composed F. Due to the defined initial frequency $f_n(0) = 50$ Hz, F can be attained. With respect to Fig. 3, point a from l_1 and point b from l_2 respectively illustrate the enhancement of droop scheme. The frequency deviation has been combined with the original reference to compose the pertinent frequency references in the points of a and b. The clue of variations in reference can be founded in the deviation between points of a and e rather in the points of b and d. The frequency reference must be adjusted from $f_n(j-1)$ to $f_n(j)$ during the load variation at j, or else, the frequency deviation of $\delta f(j)$ appears at the point of c. As a consequence, the active power variation is related to the reference variation. By adjusting the frequency reference and counteracting the frequency deviation, the final frequency has been accurately restored during the admissible active power range.

3.2. Design and analysis of restoration rate. The variation of frequency reference is here considered with additional control part $\delta f_n(t)$ to Eq. (7), i.e.:

$$\begin{aligned} f &= f_n(j) + \alpha P(j) = \\ &= \left[f_n(j-1) + \delta f_n(t) + \alpha P(j-1)\right] \end{aligned} \tag{17}$$

where, $\delta f_n(t)$ has been determined as a pertinent operator that must be stabilized during steady-state condition.

The variation rate of $\delta f_n(t)$ can be presented as follows:

$$\frac{d(\delta f_n(t))}{dt} = \gamma.\delta f(t) \tag{18}$$

where, γ indicates the frequency restoration factor, and $\delta f(t)$ indicates the variation of frequency deviation. This paper applies $\delta f_n(t)$ counteract $\delta f(t)$ toward $\delta f_n(t) = -\delta f(t)$. Therefore, the frequency deviation dynamic during the mentioned variation rate can be attained by:

$$\frac{d(\delta f(t))}{dt} = -\frac{d(\delta f(t))}{dt} = -\gamma.\delta f(t). \tag{19}$$

By solving Eq. (19), following equation is achieved:

$$\delta f(t) = -d_\delta e^{-\gamma t} \tag{20}$$

where, d_δ represents a constant value. The variation of frequency deviation has been significantly suppressed at satisfied rate via determination of the γ. Figure 4 presents the suggested frequency restoration control strategy that both the active power and frequency reference of VPP have been saved during any variation.

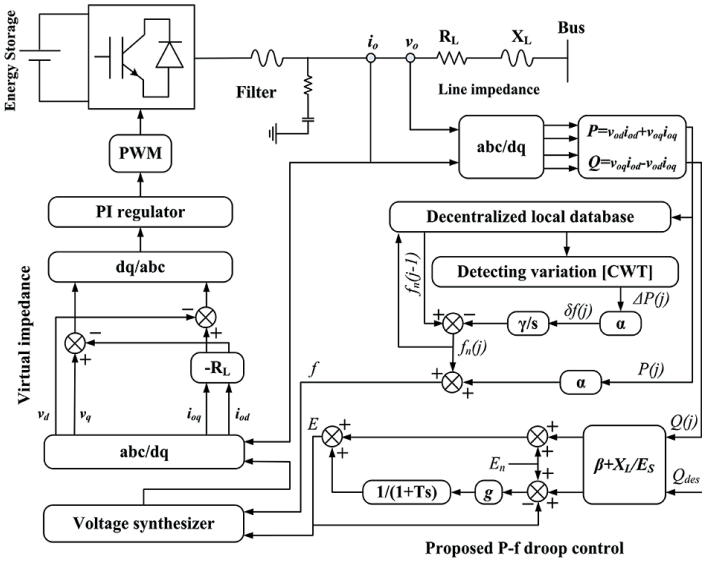

Fig. 4. Suggested decentralized control strategy for VPP

4. Suggested reactive power sharing control

The problem reactive power sharing has been here formulated which is to be correctly performed. Voltage drop of the line has been here compensated to augment the voltage droop factor. In addition, the output voltage feedback loop by means of low-pass filter has been accordingly constructed. An exact tracking performance can be attained by rational tuning the parameters.

4.1. Illustrating inaccurately the reactive power share. Two VPPs in parallel with each other connected to the microgrid have shared an identical voltage with similar nominal voltage. Therefore, substituting Eq. (6) into Eq. (7) leads to:

$$\frac{(X_{Lk}Q_k)}{E_s} - \beta_k Q_k = \frac{(X_{Ll}Q_l)}{E_l} - \beta_l Q_l. \tag{21}$$

As for the abovementioned equation, the reactive power sharing can be presented by:

$$\frac{Q_k}{Q_l} = \frac{\left(\frac{X_{Ll}}{E_s} - \beta_l\right)}{\left(\frac{X_{Lk}}{E_s} - \beta_k\right)}. \tag{22}$$

Considering Eq. (8), $\frac{\beta_k}{\beta_l} = \frac{Q_{\max,l}}{Q_{\max,k}}$ has been attained. In case of satisfying $\frac{Z_{Lk}}{Z_{Ll}} \neq \frac{\beta_l}{\beta_k}$, the following consequences have been attained:

$$\frac{Q_k}{Q_l} \neq \frac{\beta_k}{\beta_l} \quad or \quad \frac{Q_k}{Q_l} \neq \frac{Q_{\max k}}{Q_{\max l}}. \tag{23}$$

Substituting Eq. (23) into Eq. (7) for acquiring $E_k \neq E_l$, and illustrating the line impedance difference has resulted in the voltage difference and reactive power sharing inaccuracy. Fig. 5 illustrates the voltage droop scheme. l_k and l_l indicate the conventional droop curves, $l_{k'}$ and $l_{l'}$ indicate the new droop curves caused by compensating the voltage drop and enhanced voltage droop factor, E_k, E_l and Q_k, Q_l respectively indicate the output voltage and reactive power, accordingly $E_{k'}$, $E_{l'}$ and $Q_{k'}$, $Q_{l'}$ respectively indicate the required output voltage and reactive power, E_{Lk} and E_{Ll} indicate the voltage drop of the lines. Without U_{Lk} and U_{Ll}, the same $E_{k'}$, $E_{l'}$ causes the correct share of reactive power $Q_{k'}$, $Q_{l'}$ at operation points of t and u. Provided l_k and l_l have been applied to control VPP$_k$ and VPP$_l$. the inaccuracy of reactive power sharing Q_k and Q_l reveals at the operation points r and s. The voltage drop of the line has been compensated to minimize this inaccuracy.

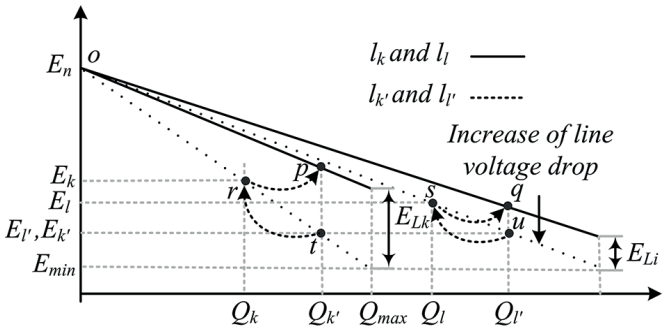

Fig. 5. Characteristics of voltage droop strategy

4.2. Modified voltage droop control by LVD. Due to inevitability of the voltage difference resulting from the voltage drop of the line, the characteristics of the voltage droop has been

increased via compensating the voltage drop that the reactive power can be accurately shared with no concern of the voltage difference. According to Fig. 5, VPP_k and VPP_l have been controlled by $l_{k'}$ and $l_{l'}$ i.e., the operation points have altered from the points of r and s to the points of p and q, accordingly the pertinent $Q_{k'}$ and $Q_{l'}$ have been attained in spite of $E_k \neq E_l$. The control equation of and can be attained via composing Eq. (6) with Eq. (7) which is:

$$\begin{aligned} E &= E_n + \left(X_L Q\right) E_s^{-1} + \beta Q = \\ &= E = E_n + \left(\beta + X_L E_s^{-1}\right) Q. \end{aligned} \tag{24}$$

Substituting Eq. (6) into Eq. (24)

$$E = E_s + \left(X_L E_s^{-1}\right) Q = E_n + \left(\beta + X_L E_s^{-1}\right) Q. \tag{25}$$

Considering VPP_k, VPP_l and $E_k \neq E_l$, Eq. (26) will be attained:

$$\frac{Q_k}{Q_l} = \frac{\beta_k}{\beta_l} \quad or \quad \frac{Q_k}{Q_l} = \frac{Q_{\max k}}{Q_{\max l}}. \tag{26}$$

Equation (26) illustrates the upgraded voltage droop approach in Eq. (24) that the reactive power has been accurately shared, whereas, eliminating the variation in actual voltages will not occur.

4.3. Output voltage feedback loop. The output voltage feedback loop has been considered for the terminal of the voltage droop to certify the voltage delivery after a satisfactory share of the reactive power. Then, appropriate feedback reference can be attained by lowpass filter. Including the feedback part, Eq. (24) of VPP will be enhanced by:

$$E_i = E_n + \left(\beta_i + \frac{X_{Li}}{E_s}\right) Q_i + g_i \frac{E_{des} - E_i}{1 + Ts} \tag{27}$$

where, g_i indicates a trivial gain, T indicates the lowpass filter time constant. $E_{\text{des},\,i}$ indicated the desirable voltage and reference of the feedback control, and can be represented by:

$$\begin{cases} E_{des,\,i} = E_n + \left(\beta_i + \dfrac{X_{Li}}{E_s}\right) Q_{des,\,i} \\ Q_{des,\,i} = \left[\dfrac{1}{\beta_i \sum_{h=1}^{N} \dfrac{1}{\beta_h}}\right] Q_l \end{cases} \tag{28}$$

where, β_h presents the voltage droop factor of VPP, N presents the number of VPPs, Q_l presents the output reactive power of VPPs, and $E_{\text{des},\,i}$ presents the desirable reactive power for satisfactory share of the reactive power. The supplemental feedback part in Eq. (27) has appropriately provided the desirable output voltage. As $E_{\text{des}i}$ to be attained for all VPPs, $Q_{\text{des}i}$ has been delivered to accurately sharing the reactive power. Eq. (27) is represented by a common droop formula, i.e.:

$$E_i = \left(E_n + \delta E_i\right) + G_i\left(\beta_i + X_{Li} E_s^{-1}\right) Q_i \tag{29}$$

where,

$$\begin{cases} \delta E_i = \dfrac{g_i}{1 + Ts + g_i} \left(\beta_i + \dfrac{X_{Li}}{E_s}\right) Q_{des,\,i} \\ G_i = \dfrac{1 + Ts}{1 + Ts + g_i} \end{cases} \tag{30}$$

The value of g_i must be highly decreased during no impact on the accuracy of the voltage tracking toward, $\delta E_i \approx 0$, $G_i \approx 1$. Therefore, the last version of Eq. (29) almost becomes Eq. (24), i.e., feedback control strategy has not approximately deteriorated the characteristics of the voltage droop.

5. Simulation

The single-line diagram of a conventional microgrid including two VPPs along with virtual inverter coupling impedance is presented in Fig. 1. All analyses have been simulated using MATLAB/SMULINK. The microgrid has been operating in the no-load condition prior to $t = 0$ s. VPPs have identically shared the overall power loads. Three scenarios are considered to analyze and evaluate the functionality of reactive power, frequency, and voltage. The conventional and suggested control strategies have been compared with each other to validate the performance of the suggested control strategy for restoring the frequency and sharing the reactive power during the load variations. Furthermore, the system stability during the VPP perturbation has been evaluated. The frequency restoration capability has been also appraised with different γ accompanied by the function of voltage feedback loop. The following scenarios have accurately analyzed the performance of proposed control strategy.

5.1. Load variation strategy. The step-up load change i.e., 25 KW + 30 KVar at $t = 1$ s is considered to reveal the performances control strategy toward frequency tracking, while the generation power is 2 MVA. By detecting the active power variation, the frequency deviation is revealed. The required reference has compensated the frequency deviation to restore the frequency. The coefficients have been promptly increased during active power variation. Defining the initial system frequency i.e., 50 Hz, matrix of frequency references has been attained with respect to Fig. 3 which illustrate the droop scheme enhancement. The frequency deviation has been combined with the original reference to compose the pertinent frequency references. By adjusting the frequency reference and counteracting the frequency deviation, the final frequency has been accurately restored during the admissible active power range. The variation of frequency deviation has been significantly suppressed at satisfied rate via of the frequency restoration factor. Based on decentralized control strategy presented in Fig. 4, both the active power and frequency references of VPP have been saved during the variation conditions. The simulation results

are provided in the Fig. 6. As for the Fig. 6a, after entrance of the load into the microgrid at $t = 1$ s, the conventional PFDC cannot restore the system frequency in its nominal value, and deviated from 50 Hz. Fallowing that, it is rested in 49.9 Hz. That is to say, the frequency deviation appears with presence of the conventional PFDC through the variation of active power. Conversely, the proposed PFDC strategy fades away the frequency deviation as shown in Fig. 6b. By compensating the variation of the frequency reference, the system frequency has been promptly retrieved into 50 Hz during load changes.

On the other hand, the voltage and reactive power sharing results are respectively presented in Figs. 7 and 8. Figures 7a and 8a present the conventional PFDC, and Figs. 7b and 8b present the suggested PFDC. According to Figs. 7a and 8a, the raise up reactive power caused by the characteristic of the voltage droop decrease the voltage. Even so, different line impedances cause appearance of voltage deference within 1.5 V. With respect to Fig. 8a, the reactive power has been inaccurately shared with presence of the conventional PFDC. The steady state value of reactive power under this variation is within 150 Var. The overall reactive powers of VPPs are lower than the load demand, which can provide system abnormality. As for Fig. 8b, both the VPPs have accurately and identically shared the reactive power i.e., 1500 Var in spite of voltage difference by means of suggested PFDC. These comparative results have essentially validated the high performance of suggested PFDC, and also the voltage feedback loop has assured the accurate share of the reactive power.

5.2. Impulsive VPP perturbation. An impulsive VPP perturbation signal has been inserted to the microgrid at $t = 1$ s. Figure 9 shows the power system responses with presence of the suggested control strategy. According to Fig. 9a, the system frequency has been promptly retrieved into 50 Hz after 0.1 s. In

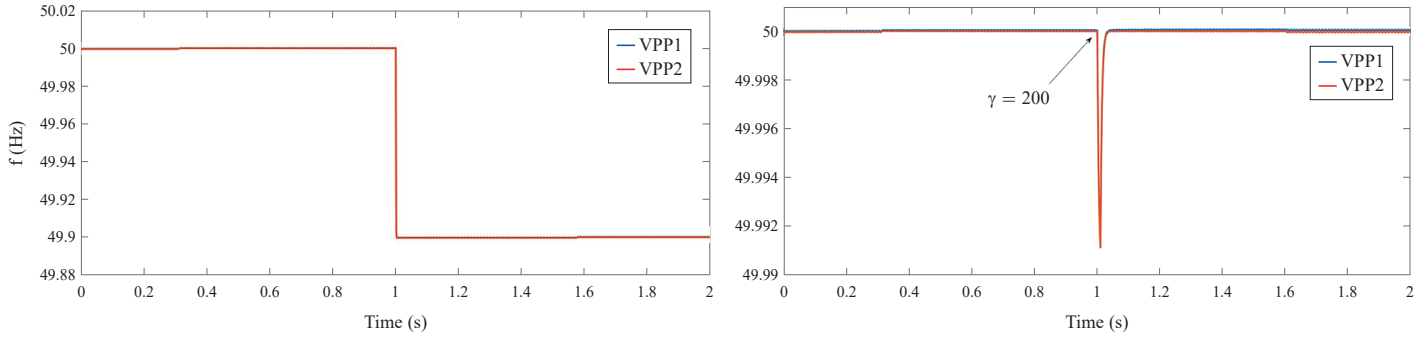

Fig. 6. Frequency responses during the step-up load change, a) with conventional PFDC, b) with proposed PFDC

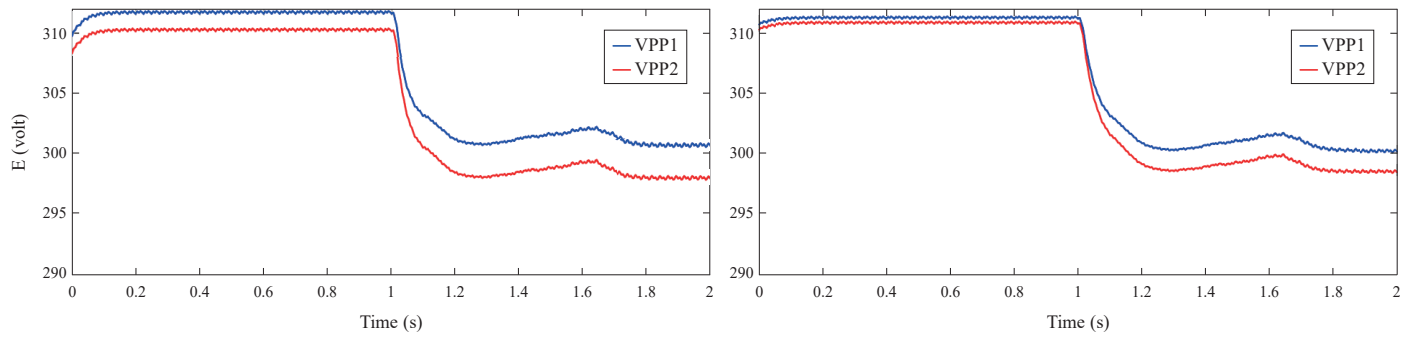

Fig. 7. Voltage response during step-up load change, a) with conventional PFDC, b) with proposed PFDC

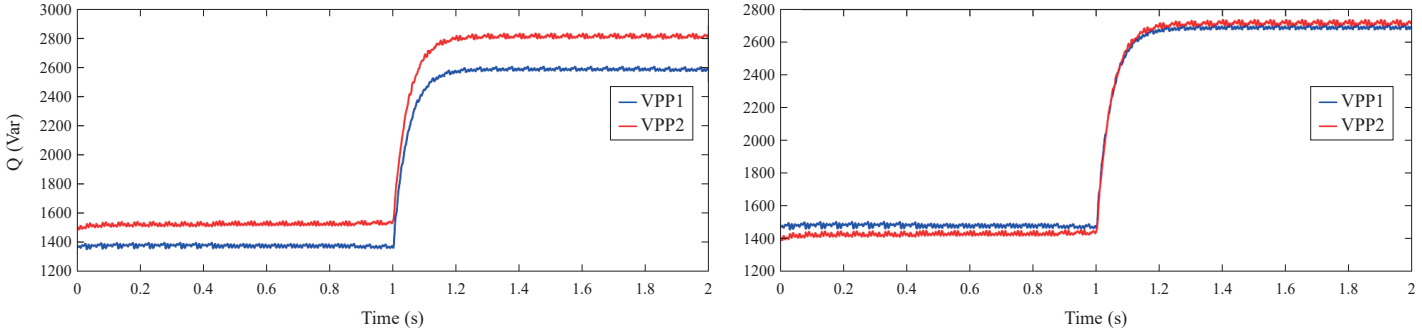

Fig. 8. Reactive power response during step-up load change, a) with conventional PFDC, b) with proposed PFDC

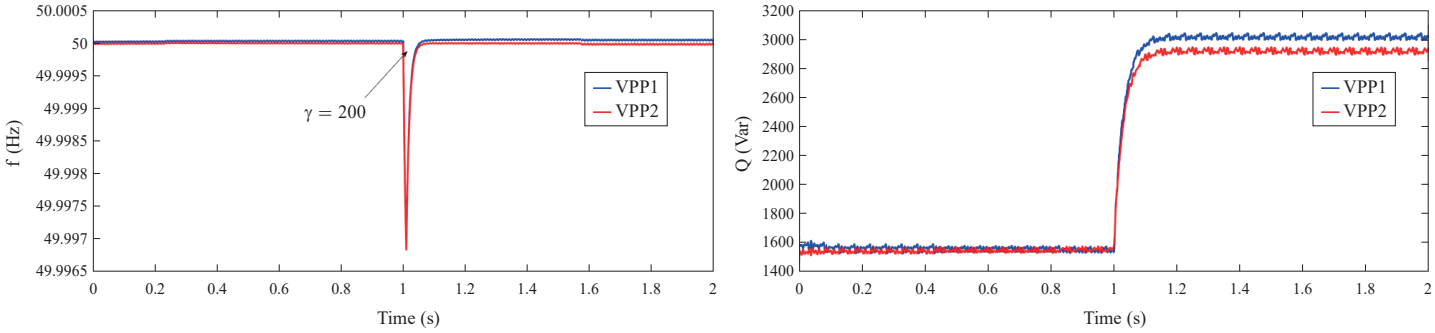

Fig. 9. Power system responses during the impulsive VPP perturbation with proposed PFDC, a) frequency, b) reactive power

addition, the effect of perturbation in the steady-state frequency restoration is very trivial. As for the 9b, the reactive power has been accurately shared, and its steady state value is not affected by perturbation. It can be concluded that the suggested control strategy has assured the prompt restoration of the system frequency and the exact share of the reactive power during the impulsive VPP perturbation.

5.3. Different values of γ. In this scenario, the values of 50 and 1200 are considered for γ to evaluate the restoration performance of the system frequency. As can be seen in Figs. 10a and 10b, the suggested control strategy with higher γ value can promptly retrieve the system frequency with much less impact. That is to say, the restoration rate of the system frequency is in proportion with γ. Therefore, high value of γ within permissible constraints provided that the restoration capability of the system frequency is not to be affected of course in the real microgrid.

6. Conclusion

In this paper, a novel upgraded droop control strategy is proposed to accurately restore the system frequency and share the reactive power in the isolated microgrids. The suggested decentralized control strategy has just modified the parameters of droop control according to the corresponding local information of the VPP. Therefore, the system did not need any communication that the reliability rate would be increased. The functionality of reactive power, frequency, and voltage has been thoroughly analyzed with consideration of three different possible scenarios. The proposed control strategy has been compared with conventional control strategy to deal with the restoration capability of the system frequency and accurate share of the reactive power during the load perturbation. By compensating the variation of the frequency reference, the system frequency has been promptly restored during the disturbed conditions. Of course, the restoration capability of the system frequency has been more enhanced by choosing large γ. Also, the reactive power has been accurately shared via droop compensation scheme. For some detailed results, the conventional PFDC cannot restore the system frequency by a load variation which reveals 0.1 deviation from 50 Hz, while proposed PFDC strategy retrieves the nominal frequency via compensating the variation of the frequency reference. Furthermore, γ exhibits its effective role to retrieve the system frequency that only a trivial transient condition with 0.001 Hz magnetite and 0.01 s duration is appeared for $\gamma = 1200$. Similar results have been obtained for other conditions.

References

[1] G.U. Atmo, C.F. Duffield, and D. Wilson, "Structuring procurement to improve sustainability outcomes of power plant projects", *Energy Technol. Policy* 2(1), 47–57 (2015).

[2] P. Kumar, P.S. Sikder, and N. Pal, "Biomass fuel cell based distributed generation system for Sagar Island", *Bull. Pol. Ac.: Tech.* 66(5), 665–674 (2018).

[3] M. Wieczorek, M. Lewandowski, and W. Jefimowski, "Cost comparison of different configurations of a hybrid energy storage system with battery-only and supercapacitor-only storage in an electric city bus", *Bull. Pol. Ac.: Tech.* 44(6), 1095–1106 (2019).

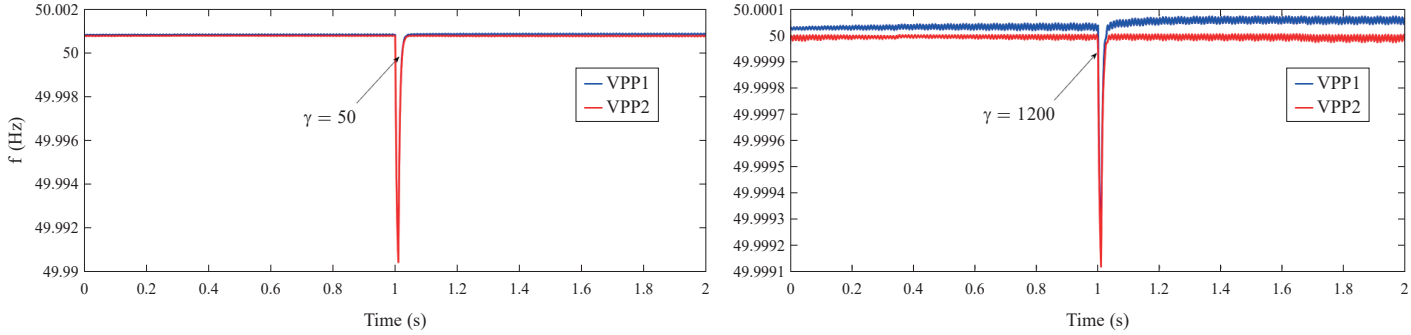

Fig. 10. Frequency responses with proposed PFDC for: a) $\gamma = 50$, b) $\gamma = 1200$

[4] W. Marańda and M. Piotrowicz, "Efficiency of maximum power point tracking in photovoltaic system under variable solar irradiance", *Bull. Pol. Ac.: Tech*. 62(4), 713–721 (2014).

[5] U. Akram, M. Khalid, and S. Shafiq, "An innovative hybrid wind-solar and battery-supercapacitor microgrid system-development and optimization", *IEEE Access* 5(10), 25897–25912 (2017).

[6] M.A. Hannan, M.G.M. Abdolrasol, M. Faisal, P.J. Ker, R.A. Begum, and A. Hussain, "Binary particle swarm optimization for scheduling MG integrated virtual power plant toward energy saving", *IEEE Access* 7(6), 107937–07951 (2019).

[7] T. Wu, Z. Liu, and J. Liu, "A unified virtual power decoupling method for droop-controlled parallel inverters in microgrids", *IEEE Trans. Power Electron.* 31(8), 5587–5603 (2016).

[8] F. Shahnia and A. Ghosh, "Coupling of neighbouring low voltage residential distribution feeders for voltage profile improvement using power electronics converters", *IET Renew. Power Gener.* 10(2), 535–547 (2016).

[9] X. Tang, X. Hu, and N. Li, "A novel frequency and voltage control method for islanded based on multienergy storages", *IEEE Trans. Smart Grid* 7(1), 410–419 (2016).

[10] H. Zhang, S. Kim, Q. Sun, and J. Zhou, "Distributed adaptive virtual impedance control for accurate reactive power sharing based on consensus control in microgrids", *IEEE Trans. Smart Grid* 8(4), 1749–1761 (2017).

[11] M. Eskandari and L. Li, "Microgrid Operation Improvement by Adaptive Virtual Impedance", *IET Renew. Power Gener.* 13(2), 296–307 (2018).

[12] Z.A. Obaid, L.M. Cipcigan, L. Abrahim, and M.T. Muhsin, "Frequency control of future power systems: reviewing and evaluating challenges and new control methods", *J. Mod. Power Syst. Clean Energy* 7(1), 9–25 (2019).

[13] R.M. Imran, S. Wang, and F.M.F. Flaih, "DQ-Voltage droop control and robust secondary restoration with eligibility to operate during communication failure in autonomous microgrid", *IEEE Access* 7(12), 6353–6361 (2019).

[14] N.N. AbuBakar, M.Y. Hassan, M.F. Sulaima, M. Na'im, M. Nasir and A. Khamisd, "Microgrid and load shedding scheme during islanded mode: A review", *Renewable Sustainable Energy Rev.*, 71(6), 161–169 (2017).

[15] T.A. Jumani, M.W. Mustafa, M.M. Rasid, N.H. Mirjat, Z.H. Leghari, and M.S. Saeed, "Optimal Voltage and Frequency Control of an Islanded Microgrid Using Grasshopper Optimization Algorithm", *Energies* 11(11), 1–20 (2018).

[16] Y. Han, P. Shen, and X. Zhao, "An enhanced power sharing scheme for voltage unbalance and harmonics compensation in an islanded AC microgrid", *IEEE Trans. Energy Convers.* 31(3), 1037–1050 (2016).

[17] M. Kosari and S.H. Hosseinian, "Decentralized reactive power sharing and frequency restoration in islanded microgrid", *IEEE Trans. Power Syst.* 32(4), 2901–2912 (2017).

[18] Y.A. Mohamed and E.F. El-Saadany, "Adaptive decentralized droop controller to preserve power sharing stability of paralleled inverters in distributed generation microgrids", *IEEE Trans. Power Electron.* 23(6), 2806–2816 (2008).

[19] X. Hou, Y. Sun, H. Han, Z. Liu, W. Yuan, and M. Su, "A fully decentralized control of grid-connected cascaded inverters", *IEEE Trans. Power Deliv.* 10(1), 315–317 (2019).

[20] L. Li, Y. Sun, Z. Liu, X. Hou, G. Shi, and M. Su, "A decentralized control with unique equilibrium point for cascaded-type microgrid", *IEEE Trans. Sustain. Energy* 10(1), 324–326 (2019).

[21] F. Guo, C. Wen, and J. Mao, "Distributed secondary voltage and frequency restoration control of droop-con-trolled inverter-based microgrids", *IEEE Trans. Ind. Electron.* 62(7), 4355–4364 (2015).

[22] S. Zuo, A. Davoudi, and Y. Song, "Distributed finite-time voltage and frequency restoration in islanded AC microgrids", *IEEE Trans. Ind. Electron.* 63(10), 5988–5997 (2016).

[23] C. Dou, Z. Zhang, and D. Yu, "MAS-based hierarchical distributed coordinate control strategy of virtual power source voltage in low-voltage microgrid", *IEEE Access* 5(1), 11381–11390 (2017).

[24] N.M. Dehkordi, N. Sadati, and M. Hamzeh, "Distributed robust finite-time secondary voltage and frequency control of islanded microgrids", *IEEE Trans. Power Syst.*, 32(5), 3648–3659 (2017).

[25] N.M. Dehkordi, N. Sadati, and M. Hamzeh, "Fully distributed cooperative secondary frequency and voltage control of islanded microgrids", *IEEE Trans. Energy Convers.* 32(2), 675–685 (2017).

[26] D.O. Amoateng, M.A. Hosani, and M.S. Elmoursi, "Adaptive voltage and frequency control of islanded multi-microgrids", *IEEE Trans. Power Syst.* 33(4), 4454–4465 (2018).

[27] Q. Shafiee, J.M. Guerrero, and J.C. Vasquez, "Distributed secondary control for islanded microgrids-a novel approach", *IEEE Trans. Power Electron.* 29(2), 1018–1031 (2014).

[28] U. Sowmmiya and U. Govindarajan, "Control and power transfer operation of WRIG-based WECS in a hybrid AC/DC microgrid", *IET Renewable Power Gener.* 12(3), 359–373 (2018).

[29] Z. Zhang, C. Dou, and D. Yu, "An event-triggered secondary control strategy with network delay in islanded microgrids", *IEEE Syst. J.* 13(2), 1851–1860 (2019).

[30] J. He and Y. Li, "An enhanced microgrid load demand sharing strategy", *IEEE Trans. Power Electron.* 27(9), 3984–3995 (2012).

[31] Y. Fan, G. Hu, and M. Egerstedt, "Distributed reactive power sharing control for microgrids with event-triggered communication", *IEEE Trans. Control Syst. Technol.* 25(1), 118–128 (2017).

[32] X. Lu. J. Lai, and X. Yu, "Distributed coordination of islanded microgrid clusters using a two-layer intermittent communication network", *IEEE Trans. Ind. Inf.* 14(9), 3956–3969 (2018).

[33] X. Wu, C. Shen, and R. Iravani, "A distributed, cooperative frequency and voltage control for microgrids", *IEEE Trans. Smart Grid*, 9(4), 2764–2776 (2018).

[34] G. Lou, W. Gu, and L. Wang, "Decentralized secondary voltage and frequency control scheme for islanded microgrid based on adaptive state estimator", *IET Gener. Transm. Distrib.*, 11(15), 3683–3693 (2017).

[35] B. Wang, S. Liu, and Y. Zhang, "Reactive power sharing control based on voltage compensation strategy in microgrid", 36th Chinese Control Conference (2017).

[36] H.E.Z. Farag, S. Saxena, and A. Asif, "A robust dynamic state estimation for droop controlled islanded microgrids", Electr. Power Syst. Res. 140(11), 445–455 (2016).

[37] K. Sabzevari, S. Karimi, F. Khosravi, and H. Abdi, "Modified droop control for improving adaptive virtual impedance strategy for parallel distributed generation units in islanded microgrids", *Int. Trans. Electr. Energy Syst.*, 29(1), e2689 (2019).

[38] C. Dou, Z. Zhang, D. Yue, and M. Song, "Improved droop control based on virtual impedance and virtual power source in low-voltage microgrid", *IET Gener. Transm. Distrib.* 11(4), 1046–1054 (2017).

[39] P.K. Ray, N. Kishor, and S.R. Mohanty, "Islanding and power quality disturbance detection in grid-connected hybrid power system using wavelet and S-transform", *IEEE Trans. Smart Grid*, 3(3), 1082–1094 (2012).